Effect of doping and elastic properties in $(Mn,Fe)_2(Si,P)$

P. Roy,[1,*] E. Torun,[2] and R. A. de Groot[2]

[1]*Institute for Molecules and Materials, Radboud University Nijmegen, Heyendaalseweg 135, 6525 AJ, Nijmegen, The Netherlands*

[2]*Department of Physics, University of Antwerp, Groenenborgerlaan 171, B-2020, Antwerp, Belgium*

(Received 9 November 2015; revised manuscript received 18 January 2016; published 25 March 2016)

Mixed magnetism (the coexistence of strong and weak magnetism in one material) is regarded as the origin of the giant magnetocaloric effect (GMCE). A good example is $(Mn,Fe)_2(Si,P)$, which is established as one of the best magnetocaloric materials available. Tuning the material properties are essential for optimizing its performance, and a straightforward way to do that is by doping. In this article, an *ab initio* electronic structure method was used to calculate the structure and magnetic properties of $3d$-transition-metal-doped $(Mn,Fe)_2(Si,P)$ materials for magnetocaloric applications (transition metals are Cr, Co, Mn, Ni, Cu). For a steady performance, the material should be mechanically stable. A detailed analysis of the elastic constants shows that the mechanical stability of the $(Mn,Fe)_2(Si,P)$ system increases significantly by doping with boron without affecting the magnetic properties. Insights of the influence of doping enable future studies to understand and predict better magnetocaloric materials.

DOI: 10.1103/PhysRevB.93.094110

I. INTRODUCTION

In recent years, the growing demand for energy has become a major concern for us. Since conventional sources of energy are limited and traditional technology has almost reached its technical boundary of energy efficiency, it is necessary to explore new potential electric devices that can overcome these challenges. Refrigeration is a major source of energy consumption in both domestic and in industrial environments. The traditional method for refrigeration has many weakness, primarily its low efficiency. Hence, more advanced methods such as *magnetic cooling*, which incorporate magnetocaloric materials, is promising. After the discovery of the giant magnetocaloric effect (GMCE) by Pecharsky and Gschneidner in $Gd_5Ge_2Si_2$ [1], room-temperature refrigeration has become a reality. During the past decade, a lot of research [2,3] has focused on this field and several classes of materials including $MnFe(P_{1-x}As_x)$[4], $La(Fe,Si)_{13}$ [5–7] and their hydrides [8] Mn(As,Sb), FeRh [9], Heusler alloys [10], and Mn_2Sb have been proposed as promising candidates for magnetic refrigerants. Some of the materials exhibiting the giant magnetocaloric effect, viz. $La(Fe,Si)_{13}$ and $MnFe(P_{1-x}T_x)$ (with T = Si, Ge, and As) can be tuned for minimal hysteresis loss around the phase transition, which is necessary for its cyclic operation. The lower hysteresis is particularly important when aiming at operations in low magnetic fields (below 1 T), making $La(Fe,Si)_{13}$- and $MnFe(P_{1-x}T_x)$- based materials most promising for real-life applications [11]. The large MCE in cubic $La(Fe,Si)_{13}$-based materials is associated with both temperature and a field-induced metamagnetic transition that comes along with a 1.5% volume change. Whereas hexagonal $MnFe(P_{1-x}T_x)$-based materials display a temperature and field-induced magneto-elastic transition that is accompanied by a significant change in the ratio c/a but hardly no change in the volume. This simultaneous occurrence of magnetic and elastic transition at the Curie temperature T_C is responsible for their enhanced performances. In last few years, further attempts were made to tune the material properties to raise the performance of these materials for better applications. For example, the Si : P ratio or the Mn : Fe ratio can be varied [12–14] to modify the transition temperature, transition order, hysteresis, crystal parameters, and magnetic properties. Similarly, different doping elements (such as Co, Ni, Cu, Cr, etc.) were used during the experiments for similar purposes [15,16]. A small amount of dopants can enhance their performance significantly without changing the stoichiometry of the lattice. An atomistic understanding of the effect of dopant on the material is required to classify better dopant and to tune the properties in a controlled way. In addition to this, the magnetocaloric material is required to be mechanically stable for sustainable repetitive operation in a magnetic cooler. The elastic properties near the phase transition play the pivotal role for their stability and brittleness. Various studies [17–20] were done previously to measure the mechanical stability of a material under stress. During the magneto-elastic transition, $(Mn,Fe)_2(Si,P)$ does not exhibit an abrupt volume change at the phase transition but only the crystal parameters change [21]. This also suggests a minor change in the volume-dependent elastic constants at T_C; however, the directional elastic constants might experience greater changes.

In this paper, we investigate the electronic structure and the magnetic properties of $(Mn,Fe)_2(Si,P)$ by using density functional theory (DFT) and the effect of doping on these properties. The results presented here will help future studies select the appropriate dopant elements for the desired magnetocaloric operations. We also evaluate the complete set of elastic parameters for boron-doped and undoped $MnFeSi_{0.33}P_{0.66}$ by applying several volume-conserved deformations. By using the values obtained from our studies we classify the materials based on their mechanical stability. Our study establishes the fact that doping with boron significantly increases the elastic constants as well as the mechanical stability of the magnetocaloric material for sustainable operation without altering the magnetic properties.

*p.roy@science.ru.nl

II. DETAILS OF CALCULATION

We performed density functional theory calculations by using the Vienna *ab initio* simulation package (VASP) [22], employing the projector augmented wave (PAW) method. Exchange interactions were taken into account by using the generalized gradient approximation (GGA) by Perdew, Burke, and Ernzerhof (PBE) [23]. For all the calculations, PAW data sets were used with $1s$, $2s$, $2p$, and $3s$ core states frozen for Mn. In Fe atoms, an additional $3p$ semicore state was kept frozen, since it lies deeper in energy. For Si and P, $1s$, $2s$, and $2p$ core states were kept frozen. For the Brillouin zone integration we used a Γ-centered k-point mesh of $3 \times 3 \times 10$ points in the irreducible part of the Brillouin zone. The energy cutoff of the plane-wave function is taken at 500 eV, and for smearing a Gaussian function with smearing width of 0.05 eV was employed. The atomic positions were relaxed for all the calculations with a criterion for the force convergence of 1 meV/Å for the atoms. The energies and eigenvalues were converged to 0.01 meV. The $(Mn,Fe)_2(Si,P)$ series of materials has a layered hexagonal structure (space group $189/P\bar{6}2m$). Fe and Mn atoms prefer to occupy 3f and 3g sites [24] and Si and P atoms usually occupy 2c and 1b sites [25], respectively (Fig. 1). These Wyckoff sites containing Mn and Fe atoms comprise two parallel alternating layers. Both the Mn and Fe atoms are magnetic and Dung *et al.* [12] have explained the behavior of individual atoms within the crystal. It was shown that Mn and Fe behave as strong and weak magnets, respectively, within the lattice; i.e., the magnetic moment rearranges for the Mn atoms but vanishes in case of Fe atoms during a ferromagnetic (FM) to paramagnetic (PM) phase transition. Since both of these elements are transition metals located in the third row of the periodic table, other $3d$-transition-metal elements were chosen for doping (Cr, Mn, Co, Ni, Cu at the 3f site and Co, Ni, Cu at the 3g site) without deforming the crystal structure substantially. For obtaining a systematic understanding of the effect of dopant atoms within the crystal structure, charge density differences were plotted and the occupation of electron orbitals was calculated.

An antiparallel magnetic ordering with a $1 \times 1 \times 2$ supercell is used as an approximation to model the PM phase for the undoped system. The moments of the atoms within the same unit cell remain constant and an alternating arrangement of spin-up and spin-down moments were used along the z direction; for details see the supplemental material [26]. This approximation worked well with this series of materials, as proved in Sec. IV. We have chosen $MnFeSi_{0.66}P_{0.33}$ stoichiometry for the calculations with a 1 : 1 and 2 : 1 ratio for the metallic and nonmetallic atoms, respectively, to distinguish the crystallographic sites with the chemical species. The undoped unit cell of $MnFeSi_{0.66}P_{0.33}$ is composed of nine atoms and the lattice parameters are $a_{\text{fer}} = 6.16$ Å, $c_{\text{fer}} = 3.25$ Å in the FM state and $a_{\text{para}} = 6.08$ Å, $c_{\text{para}} = 3.47$ Å in the PM state as obtained from the optimization of the crystal parameters. This matches well with the experiments [16]. The point group symmetry reduces from D_{3h} to C_{3v} due to the flipping of moments between nearest unit cells in the $1 \times 1 \times 2$ supercell. Since a small amount of doping (8%) will not change the lattice parameters significantly, we kept the optimized lattice parameters the same throughout our calculation after doping. We created a $2 \times 2 \times 1$ supercell with one dopant atom replacing Mn or Fe at the 3g or 3f sites, respectively, in the FM state. The PM phase is modeled by doubling that FM supercell with antiparallel ordering along the z direction to make the total moment zero (see supplemental material [26])]. The lattice parameters for this $2 \times 2 \times 2$ supercell are taken from the optimized undoped unit cell. For both magnetic cases, the atomic positions were relaxed with the force and energy convergence criteria specified before.

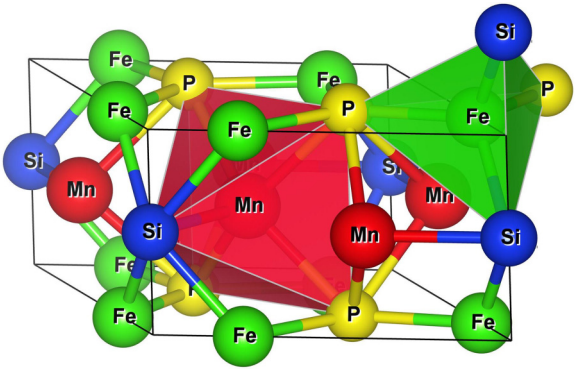

FIG. 1. Schematic representation of $MnFeSi_{0.33}P_{0.66}$ unit cell. Mn and Fe atoms are placed at 3g (square pyramidal, red) and 3f (tetrahedral, green) crystallographic sites, respectively.

III. RESULTS AND DISCUSSIONS

A. Effects of doping

In the FM state of undoped $MnFeSi_{0.66}P_{0.33}$, the local moments of Fe and Mn are $1.509\mu_B$ and $2.823\mu_B$, respectively. In the PM state the local moments of Fe and Mn are $0.695\mu_B$ and $2.805\mu_B$, respectively. These values of local (and total) magnetic moments directly influence the magnetocaloric properties and can be tuned by doping with other magnetic atoms from the $3d$ transition-metal row. In the first case of doping, an Fe atom at the 3f Wyckoff position is replaced by a Cr, Mn, Co, Ni, or Cu atoms. It is predicted in our calculation (see Table I) that the local magnetic moments of the dopant atoms (Cr to Cu) at the 3f site are lower than that of the Fe atoms at the same site and ranging from $0.930\mu_B$ to $0.008\mu_B$ in the FM state. This is a consequence of the fact that the number of valence electrons increase from left to right in the periodic table and hence the magnitude of magnetic moment decreases. The Cr-doped sample is interesting in particular, since the direction of magnetic moment of the Cr atom is antiparallel to the other Fe atoms in the unit cell. However, in all other cases of doping, the magnetic moment of the dopant atoms are parallel to the Fe moment within the 3f plane. The local moment of all the magnetic atoms increase with doping ranging from Cr to Cu. The $3d$ shell of the Cr atom is largely unoccupied while for Cu it is almost filled; hence, Cr is more prone to bonding compared to Cu with neighboring Fe or Mn atoms. Considering that the chemical bonding competes with magnetism, the polar-covalent bond with the Mn or Fe atoms in Cr-doped sample shows a lower magnetic moment than that in the Cu-doped sample. Cu has the weakest bond; which in

TABLE I. The local and total magnetic moment and energy calculated per formula unit (f.u.) for $MnFe_{0.92}T_{0.08}Si_{0.66}P_{0.33}$ where T = Cr, Mn, Co, Ni, and Cu in both ferromagnetic and paramagnetic configurations replace Fe atom at the 3f Wyckoff site.

	FM moment μ_B/f.u.	PM moment μ_B/f.u.	PM-FM energy eV/f.u.
$MnFe_{0.92}Cr_{0.08}Si_{0.66}P_{0.33}$			
Mn (3g)	2.797	2.793	
Fe (3f)	1.461	0.541	
Cr (3f)	−0.930	1.796	
Total	3.966	0.004	0.260
$Mn_{1.08}Fe_{0.92}$ $Si_{0.66}$ $P_{0.33}$			
Mn (3g)	2.802	2.798	
Fe (3f)	1.491	0.629	
Mn (3f)	0.718	2.170	
Total	4.129	0.000	0.259
$MnFe_{0.92}Co_{0.08}Si_{0.66}P_{0.33}$			
Mn (3g)	2.838	2.815	
Fe (3f)	1.525	0.802	
Co (3f)	0.587	0.017	
Total	4.185	0.001	0.267
$MnFe_{0.92}Ni_{0.08}Si_{0.66}P_{0.33}$			
Mn (3g)	2.853	2.826	
Fe (3f)	1.556	0.710	
Ni (3f)	0.168	0.003	
Total	4.195	0.000	0.262
$MnFe_{0.92}Cu_{0.08}Si_{0.66}P_{0.33}$			
Mn (3g)	2.859	2.823	
Fe (3f)	1.575	0.551	
Cu (3f)	0.008	0.002	
Total	4.206	0.000	0.244

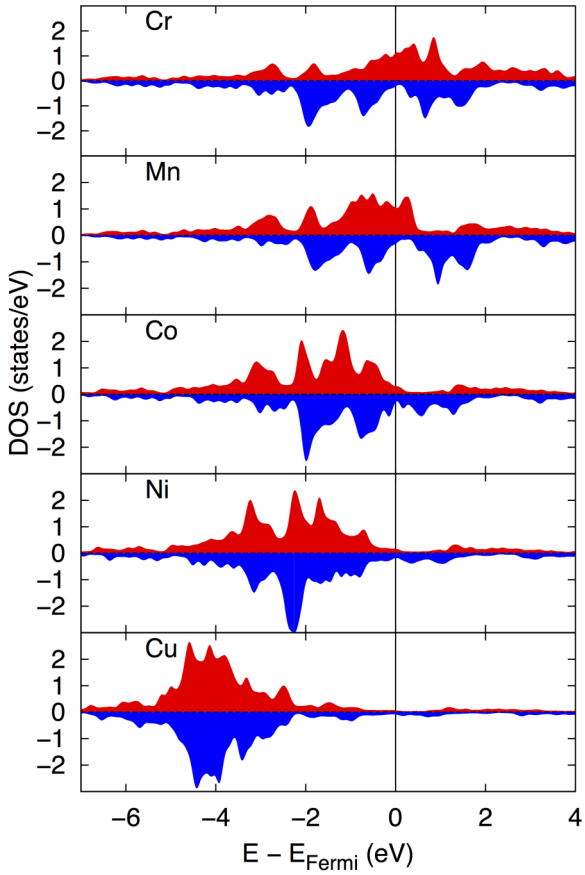

FIG. 2. Partial density of states of T = Cr, Mn, Co, Ni and Cu in $MnFe_{0.92}T_{0.08}Si_{0.66}P_{0.33}$ compounds in the ferromagnetic phase. Zero corresponds to the Fermi energy (E_{Fermi}). The red and blue correspond to the spin-up and spin-down states, respectively.

turn enhances local moments of the neighboring atoms and henceforth the total moment.

There are certain trends that we observe from the density of states (DOS) pictures (see Fig. 2). The partial density of states (pDOS) for all the dopant atoms within the unit cell of $MnFe_{0.92}T_{0.08}Si_{0.66}P_{0.33}$ are shown. As the empty $3d$ shells are filling up (top to bottom of Fig. 2), the states above the Fermi energy decrease and the DOS shifts towards lower energy.

In the second set of calculations, the Mn atom at the 3g site is replaced with Co, Ni, and Cu with the FM and PM configurations. Changing the dopant atoms from Co to Cu, the local as well as total magnetic moment declines as the number of unfilled $3d$ orbitals decreases. The local moment of the dopant atoms at the 3g sites (see Table II) are marginally higher than that in the 3f sites, as shown in Table I.

This can be explained on the basis of the nearest-neighbor distances. The 3f site is tetragonal whereas the 3g site is square pyramidal with nearest-neighbor distances of 2.26 and 2.46 Å, respectively. Therefore the dopant elements at the 3g site have lesser bonding probability as compared to those at the 3f site. As a result, the local moment at the 3f position is comparatively smaller than that in the other site for the same element. For the same reason, Mn and Fe atoms in $Mn_{0.92}T_{0.08}FeSi_{0.66}P_{0.33}$ have lesser fluctuation in their local moment values with various doping compared to those shown in Table I. We noted from

TABLE II. The local and total magnetic moment and energy calculated per f.u. for $Mn_{0.92}T_{0.08}FeSi_{0.66}P_{0.33}$ where T = Co, Ni, Cu in both ferromagnetic and paramagnetic configurations replace the Mn atom at the 3g Wycloff site.

	FM moment μ_B/f.u.	PM moment μ_B/f.u.	PM-FM energy eV/f.u.
$MnFe_{0.92}Co_{0.08}Si_{0.66}P_{0.33}$			
Mn (3g)	2.848	2.837	
Fe (3f)	1.523	0.809	
Co (3g)	0.989	0.705	
Total	4.118	0.000	0.763
$Mn_{0.92}Ni_{0.08}FeSi_{0.66}P_{0.33}$			
Mn (3g)	2.863	2.835	
Fe (3f)	1.558	4.115	
Ni (3g)	0.322	0.196	
Total	4.115	0.000	0.765
$Mn_{0.92}Cu_{0.08}FeSi_{0.66}P_{0.33}$			
Mn (3g)	2.849	2.815	
Fe (3f)	1.523	0.802	
Cu (3g)	0.023	0.017	
Total	4.041	0.001	0.267

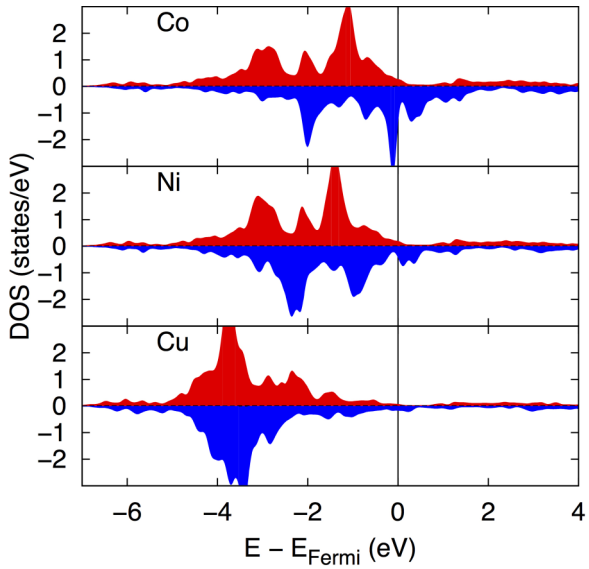

FIG. 3. Partial density of states of T = Co, Ni and Cu in $Mn_{0.92}T_{0.08}FeSi_{0.66}P_{0.33}$ compounds in the ferromagnetic phase. Zero corresponds to the Fermi energy (E_{Fermi}). The red and blue correspond to the spin-up and spin-down states, respectively.

Tables I and II that the local moment of the same dopant elements are relatively larger in the 3g site compared to the 3f site and that the pDOS (Figs. 2 and 3) is more localized below the Fermi energy. A sizable difference is observed when we compared the change in local moments for each dopant atoms from the FM to PM state. The magnetic moments of these atoms at the 3f site change significantly (70%–100%) during the phase transition whereas the same elements at the 3g site show rather smaller (25%–40%) change. This observation suggested that the strong or weak magnetic behavior is more of a site-dependent property rather than an element-specific property.

B. Charge density difference and *d*-orbital occupancy

To explain the insight of the effect of doping, we plotted the electron-density differences for the compounds. The charge densities were calculated for both the FM and PM phases, respectively. Then the latter is subtracted from the FM charge density. We noticed that the change in the charge density is much smaller in the 3g plane compared with the 3f plane, so we have shown only the 3f planes for all three cases of doping (Fig. 4). This change in charge density is responsible for the change in chemical bonding that initiates the magneto-elastic transition [12]. In Figs. 4(a) and 4(b), the highlighted section around the Cr and Mn sites have similar characteristics of charge density while the Co site shows some differences. This can be explained by bonding characteristics of the dopant atom with its neighbors. The charge density depletes between Si and T (=Cr, Mn) atoms for FM-to-PM transition leading to the decline of bonding strength between them. Since chemical bonding and magnetic moments are competing with each other, the magnetic moment increases for those two dopant atoms during that transition, as shown in Table I.

Since the dopant elements used in this present discussion are 3d elements with a nonzero DOS near the Fermi energy (see Fig. 2), the magnetic properties and bonding with the neighboring atoms are primarily governed by the 3d electrons. In this study, we calculated the occupation number of all individual 3d orbitals in both the FM and PM phases. In Fig. 4 we observe that, at the doping site, two different sets of orbitals are centered around the dopant atom. Since the p-orbital occupancy does not change with the phase transition, these orbitals are 3d orbitals. Comparing with Table III and Fig. 4 we find that the orbital with four lobes (red around Cr and Mn and blue around Co) is the d_{zx} orbital. Similarly, in Table III the 3d orbital occupation numbers suggest that the blue orbitals around Cr and Mn atoms are d_{z^2} orbitals.

The highlighted orbitals around Co atom, as shown in Fig. 4(c), are same in appearance as the rest of the Fe atoms within the plane; however, the change in orbital occupation

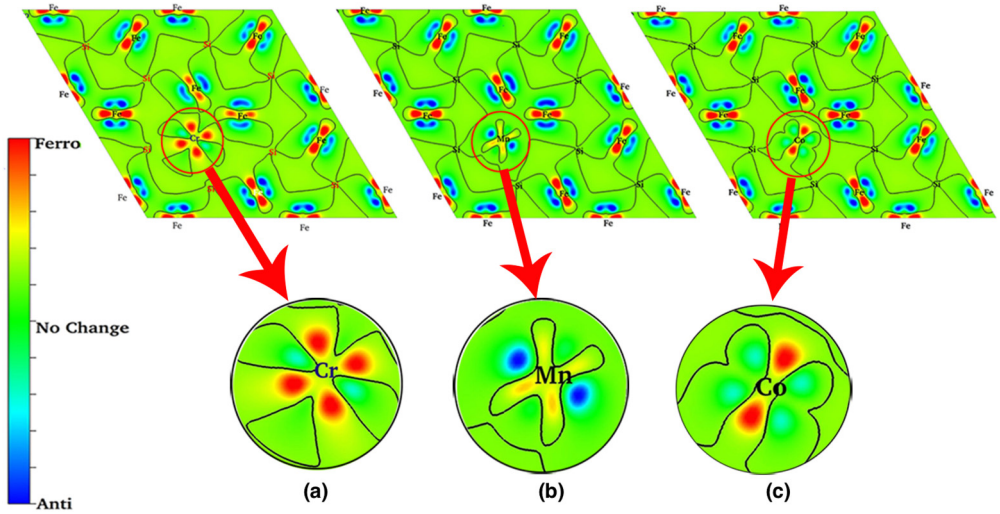

FIG. 4. Charge-density-difference plots for (a) Cr-doped, (b) Mn-doped, and (c) Co-doped samples. Paramagnetic charge density is subtracted from ferromagnetic charge density. The color scheme is red for positive charge density and blue for negative charge density. The black lines correspond to isosurfaces with no change in electron densities. The insets show the charge density around the dopant atoms in all three cases.

TABLE III. The d-orbital occupancy of T (=Co, Cr, Mn) in $MnFe_{0.92}T_{0.08}Si_{0.66}P_{0.33}$ for both ferromagnetic (FM) and paramagnetic (PM) configurations.

	d_{xy}	d_{yz}	d_{zx}	d_{z^2}	$d_{x^2-y^2}$
Co-FM	1.511	1.453	1.523	1.469	1.445
Co -PM	1.487	1.445	1.554	1.438	1.473
Mn -FM	1.051	1.041	1.084	0.983	1.032
Mn -PM	1.031	1.062	0.960	1.062	1.060
Cr -FM	0.885	0.945	0.815	0.874	0.981
Cr -PM	0.927	0.995	0.752	0.921	0.936

is much less pronounced during the FM-to-PM transition. It indicates a smaller change in the local magnetic moment for Co atoms compared to Fe atoms (see Table I). In all the above-discussed cases, doping at the Fe sites leads to the devaluation of local magnetic moment, which affects the magnetocaloric materials.

IV. ELASTIC PROPERTIES

The elastic properties for the polycrystalline magnetocaloric materials are important because of their relation to the mechanical stability of the system. During the simultaneous elastic and magnetic transition at T_C, the material remains stable if it exhibits a minimal change in crystal-structure parameters and has higher elastic constants. An understanding is essential of the relation between the elastic constants and their mechanical stability for the magnetocaloric material and also of the influence of suitable dopant material (viz. boron) on the elastic properties. Boron is a nonmagnetic semimetal and can be placed in a nonmagnetic (2c or 1b site) site with a significant influence in the elastic properties but with hardly no affect on the magnetic properties. Studies have been carried out previously to find the elastic constants of several systems by using DFT [18–20]. Since MnFeSiP systems have a hexagonal crystal structure, there are five independent elastic constants to construct the full elastic-constant matrix [27,28]. Using those directional elastic constants, we calculated the polycrystalline elastic constants by using the Voigt or Reuss assumptions [29].

First we optimized the structure of $MnFeSi_{0.33}P_{0.66}$ using VASP [22] for both ferromagnetic and paramagnetic phases.

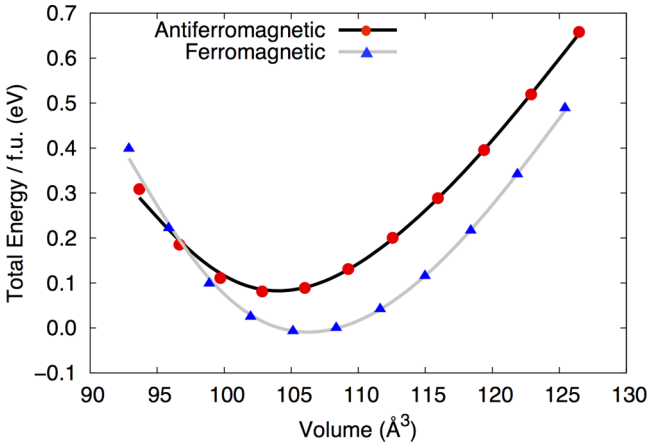

FIG. 5. Total energy per formula unit as a function of volume per unit cell for $MnFeSi_{0.33}$ $P_{0.66}$ in FM and PM states. The energy scale has been shifted to the energy minima in the FM state. The parabolas are fit with the Murnaghan equation of state [30]. The bulk moduli are calculated from the slope.

Then, starting from these equilibrium structures, the volume of the unit cell is varied in small steps. For every such step, the lattice parameters and the ionic positions of the lattice are optimized with energy- and force-convergence criteria of 10^{-5} eV/atom and 0.005 eV/Å, respectively. By using the relation for an isotropic lattice, $B_v = -V_0 \partial^2 E/\partial V^2$, the bulk modulus is obtained for both of the magnetic states. From Fig. 5, the optimized volume in ferromagnetic and paramagnetic states is obtained as 106.06 and 103.54 Å^3 with the c/a ratio of 0.495 and 0.566, respectively. The bulk modulus changes from 184.30 to 177.44 GPa during the ferromagnetic-to-paramagnetic phase transition. Although the c/a ratio is estimated below the experimentally obtained value, the increment from ferromagnetic to paramagnetic transition is consistent with experiment. The bulk modulus values suggest that the ferromagnetic state is elastically more stable than the paramagnetic phase.

In an alternative method, the energy is calculated from multiple sets with different lattice parameters. The atomic positions are optimized for every such individual calculation.

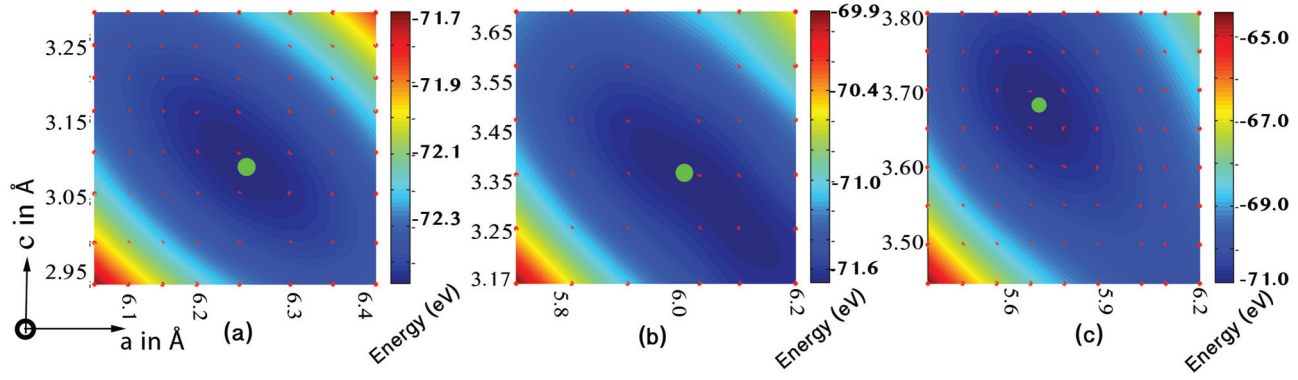

FIG. 6. Lattice parameter as a function of total energy per unit cell for $MnFeSi_{0.33}P_{0.66}$ in (a) ferromagnetic, (b) paramagnetic, and (c) nonmagnetic cases. The red dots correspond to the data obtained from the calculations, and the paraboloids were fit to those points by using a fourth-order polynomial. The green dots represent the minimum-energy points on the paraboloid, representing the equilibrium lattice constants.

TABLE IV. Local and total magnetic moment (in μ_B/f.u.) for $MnFeSi_{0.33}P_{0.66}$ and $MnFeSi_{0.33}P_{0.58}B_{0.08}$ in ferromagnetic (FM) and paramagnetic (PM) states.

	$MnFeSi_{0.33}P_{0.66}$		$MnFeSi_{0.33}P_{0.58}B_{0.08}$	
	FM	PM	FM	PM
Mn	2.895	2.884	2.875	2.862
Fe	1.549	0.683	1.526	0.675
B			− 0.196	− 0.015
Total	4.350	0.001	4.297	0.000

In Fig. 6, the total energy as a function of lattice parameters is plotted. The minima of the paraboloid gives the optimized value of the lattice parameters. Thus, in the ferromagnetic phase, the equilibrium lattice parameters obtained are $a = 6.25$ Å, $c = 3.12$ Å. To model the paramagnetic phase, we conducted two separate sets of calculations. In the first case, a nonmagnetic calculation is performed and the lattice parameters $a = 5.75$ Å and $c = 3.55$ Å are obtained. In the other case, a paramagnetic configuration is chosen and $a = 6.01$ Å, $c = 3.42$ Å are obtained. The values of lattice parameters in the FM and PM states are close to experiment with a similar trend (FM: $a = 6.17$ Å, $c = 3.28$ Å; PM: $a = 6.02$ Å, $c = 3.48$ Å) [16]. This makes the PM configuration a better approximation to model the paramagnetic state compared to the nonmagnetic calculation. In a similar graph of energy versus lattice parameter, the semimajor axis of the paraboloid would make a 45° angle with both the a and c directions for isotropic cubic material. And in an extremely anisotropic material like graphite where the atomic interaction along the c direction is negligible compared with that within the a-b plane, the semimajor axis is almost parallel to the c direction [20]. From the shape of the paraboloid as projected on the a-c plane in Fig. 6, it can be identified that the anisotropy is along the c direction; however, the anisotropy is well below that of graphite.

The hexagonal lattice has five independent elastic constants which can be calculated by applying volume-conserved deformations along the certain crystal directions specified by Lars Fast *et al.* [27] The directional elastic constants are calculated for $MnFeSi_{0.33}P_{0.66}$ after optimizing the equilibrium volume of the unit cell for both ferromagnetic and paramagnetic alignment. Recently F. Guillou *et al.* found experimentally that a small amount of boron doping enhances the mechanical stability of the MnFeSiP system while keeping the magnetocaloric properties intact [31–33]. To understand the effect of doping on elastic properties of the MnFeSiP-based systems, 8% boron was doped at the nonmagnetic site by substituting a Si atom. The volume and the lattice parameters of the unit cell are optimized for $MnFeSi_{0.33}P_{0.58}B_{0.08}$. The local and the total magnetic moments are listed in Table IV for both undoped and boron-doped systems. Boron is a nonmagnetic atom, and it was chosen to be placed at the nonmagnetic 2c site. As a result, the boron carries very small induced magnetic moment in the FM phase that vanishes in the low-moment phase. It is important to notice from Table IV that boron doping has minimal influence on the total magnetic moment of the unit cell (reduces by ≈1.2%). However, this small amount of doping significantly modifies the elastic properties of the systems, which is essential to obtain the mechanical stability of the material without compromising the magnetocaloric effect. It was also noted that the nearest Fe atoms to the dopant atoms gain ≈3% moments, while the nearest Mn atoms lose ≈1% local moments.

In Table V the elastic constants for these two systems in both FM and PM phases are listed; they are obtained by applying the volume-conserved deformation to the unit cell. However, for a polycrystalline sample, the polycrystalline bulk modulus (B), shear modulus (G) are determined by using the Voigt and Reuss assumptions (Table VI). In the Voigt assumption, the uniform strain in the polycrystalline sample was equated to the external strain and in Reuss assumption; the uniform stress was balanced with external stress. By using energy considerations, Hill later proved that these two assumptions represent the upper and lower limit for a true polycrystalline constant and an arithmetic mean would represent the true value [29]. The Young modulus (Y) and the Poisson's ratio (σ) were also calculated according to Hill's method. From the calculated elastic constants we further determined Debye temperature (θ_D) [34], which correlates with the physical properties of the solid; for example, specific heat, melting temperature, etc. Below θ_D, there is no difference between the adiabatic and isothermal elastic constants. Within this low-temperature limit, the vibrational excitations originate from acoustic vibrations; so θ_D calculated from elastic constants is the same as that obtained from the specific-heat data. In Table VI the values of B_H, G_H, and Y_H for $MnFeSi_{0.33}P_{0.66}$ are lower than that of $MnFeSi_{0.33}P_{0.58}B_{0.08}$ for the FM and PM states, respectively. This suggests that doping with boron increases the resistance of the material against deformation, thus giving enhanced mechanical stability to the system. The bulk modulus as calculated from the volume deformation using the isotropic lattice assumption and that of the polycrystalline Voigt assumption gives comparable values for $MnFeSi_{0.33}P_{0.66}$. The Debye temperature as evaluated in Table VI is sufficiently

TABLE V. Directional elastic constants (in eV/Å^3) for $MnFeSi_{0.33}P_{0.66}$ and $MnFeSi_{0.33}P_{0.58}B_{0.08}$ in ferromagnetic (FM) and paramagnetic (PM) states.

	$MnFeSi_{0.33}P_{0.66}$		$MnFeSi_{0.33}P_{0.58}B_{0.08}$	
	FM	PM	FM	PM
C_{11}	1.925	1.850	2.046	1.888
C_{12}	0.749	0.677	0.804	0.672
C_{13}	0.899	0.841	0.983	0.831
C_{33}	1.422	1.812	1.509	1.798
C_{55}	0.746	0.703	0.791	0.722

TABLE VI. Polycrystalline bulk modulus (B in GPa) and shear modulus (G in GPa) under Voigt, Reuss, and Hill assumptions. Young modulus (Y in GPa), Poisson's ratio (σ) and Debye temperature (θ_D in K) with the Hill's assumption for $MnFeSi_{0.33}P_{0.66}$ and $MnFeSi_{0.33}P_{0.58}B_{0.08}$ in ferromagnetic (FM) and paramagnetic (PM) states.

	B_V	B_R	B_H	G_V	G_R	G_H	Y_H	σ_H	θ_D
$MnFeSi_{0.33}P_{0.66}$ (FM)	184.62	182.32	186.08	95.69	86.70	91.19	235.07	0.286	544.24
$MnFeSi_{0.33}P_{0.66}$ (PM)	164.31	181.91	173.11	87.40	95.81	91.61	233.61	0.284	552.76
$MnFeSi_{0.33}P_{0.58}B_{0.08}$ (FM)	198.43	196.08	197.25	100.92	90.20	95.56	246.74	0.292	556.49
$MnFeSi_{0.33}P_{0.58}B_{0.08}$ (PM)	182.42	182.36	182.39	100.41	97.99	99.20	251.92	0.269	563.78

larger than that of T_C of the respective systems, indicating that the calculated polycrystalline elastic constants for both the FM and PM states shall be comparable to the elastic constants obtained from the specific-heat data.

According to Pugh [35], B measures the resistance to fracture and G represents its resistance towards plastic deformation. So a ratio of B/G determines the ductility and brittleness of the corresponding material. The critical value of 1.75 separates these two kinds. A value above (below) 1.75 represents ductility (brittleness). For example, the B/G ratio of steel (ductile) and glass (brittle) are 2.01 and 1.33, respectively. For $MnFeSi_{0.33}P_{0.66}$ (in Table VI), the ratio is 2.04 in the FM phase and 1.88 in the PM phase and, for $MnFeSi_{0.33}P_{0.58}B_{0.08}$, the ratio is 2.06 and 1.84, respectively, for the FM and PM phases. These values clearly suggest that the material under discussion exhibits ductility, which reduces during a phase transition from the ferromagnetic to the paramagnetic phase. The Poisson ratio is just above the lower limit (0.25) of central force solid and higher values represent directional bonding.

V. CONCLUSIONS

In this article, we discuss the effect of doping by various $3d$ transition metals on the magnetic properties of $MnFeSi_{0.66}P_{0.33}$. A clear and complete explanation of the change in electronic and magnetic properties is provided by analyzing the electronic structure around the dopant atoms. We show how different $3d$-transition-metal atoms in the series bond with neighboring atoms in both 3f and 3g crystallographic sites. The charge-density plot and the following analysis based on the d-orbital occupation numbers help us to identify the orbital structure and its influence on chemical bonding. The size of the magnetocaloric effect, as measured by quantities such as latent heat and ΔT_{ad} (adiabatic temperature change) depend on the magneto-elastic transition. And the latent heat in this magneto-elastic transition has electronic and magnetic contributions and elastic transitions [7]. This study accompanied by experiments will help in the understanding of the interconnection between the change in magnetic properties and the size of the magnetocaloric effect.

We studied the elastic properties and the mechanical stability of magnetocaloric materials, which are essential for determining the long-term applicability in a magnetic refrigerator, and the effect of doping on them. A good magnetocaloric material, which can be used with a repeating magnetization and demagnetization cycle, must exhibit mechanical stability at temperatures around its phase transition. Both lattice structure and the crystallinity of GMC materials determine this. We presented a complete documentation of the crystalline and polycrystalline elastic constants, which decide this mechanical stability of the material. The individual directional and polycrystalline elastic constants are within an implicit error of 10% for the DFT calculations [36]. In our calculation, we found the relatively high values of elastic constants that are essential for resistance against deformation. Our study conclusively shows that doping with boron significantly increases the elastic constants and hence the mechanical stability of magnetocaloric material without compromising the magnetic properties (Table IV), which is essential for its sustainable operation.

ACKNOWLEDGMENTS

This work is part of an Industrial Partnership Programme (IPP I28) of Fundamenteel Onderzoek der Materie (FOM) (The Netherlands) and co-financed by BASF New Business. The authors would like to thank Phuong Thao Nguyen and Dr. Gilles A. de Wijs for very useful discussions.

[1] V. K. Pecharsky and K. A. Gschneidner, Jr., Phys. Rev. Lett. **78**, 4494 (1997).

[2] A. Smith, C. R. H. Bahl, R. Bjork, K. Engelbrecht, K. Nielson, and N. Pryds, Adv. Energy Mater. **2**, 1288 (2012).

[3] E. Brück, *Handbook of Magnetic Materials*, edited by K. H. J. Buschow (Elsevier, Amsterdam, 2008), Vol. 17, p. 235.

[4] O. Tegus, E. Brück, K. H. J. Buschow, and F. R. de Boer, Nature (London) **415**, 150 (2002).

[5] O. Gutfleisch, A. Yan, and K. H. Muller, J. Appl. Phys. **97**, 10M305 (2005).

[6] M. K. Han and G. J. Miller, Inorg. Chem. (Washington, DC, U. S.) **47**, 515 (2008).

[7] M. E. Gruner, W. Keune, B. Roldan Cuenya, C. Weis, J. Landers, S. I. Makarov, D. Klar, M. Y. Hu, E. E. Alp, J. Zhao, M. Krautz, O. Gutfleisch, and H. Wende, Phys. Rev. Lett. **114**, 057202 (2015).

[8] A. Fujita, S. Fujieda, Y. Hasegawa, and K. Fukamichi, Phys. Rev. B **67**, 104416 (2003).

[9] M. Manekar and S. B. Roy, J. Phys. D: Appl. Phys. **41**, 192004 (2008).

[10] T. Krenke, E. Duman, M. Acet, E. F. Wassermann, X. Moya, L. Mañosa, and A. Planes, Nat. Mater. **4**, 450 (2005).

[11] E. Brück, J. Phys. D: Appl. Phys. **38**, R381 (2005).

[12] N. H. Dung, Z. Q. Ou, L. Caron, L. Zhang, D. T. Cam Thanh, G. A. de Wijs, R. A. de Groot, K. H. J. Buschow, and E. Brück, Adv. Energy Mater. **1**, 1215 (2011).
[13] N. H. Dung, L. Zhang, Z. Q. Ou, and E. Brück, Appl. Phys. Lett. **99**, 092511 (2011).
[14] N. H. Dung, L. Zhang, Z. Q. Ou, and E. Brück, Scr. Mater. **67**, 975 (2012).
[15] E. Brück, N. Trung, Z. Ou, and K. Buschow, Scr. Mater. **67**, 590 (2012).
[16] Z. Ou, Ph.D. thesis, Delft University of Technology, 2013.
[17] Z. Gercsi, E. K. Delczeg-Czirjak, L. Vitos, A. S. Wills, A. Daoud-Aladine, and K. G. Sandeman, Phys. Rev. B **88**, 024417 (2013).
[18] R. Stadler, W. Wolf, R. Podloucky, G. Kresse, J. Furthmüller, and J. Hafner, Phys. Rev. B **54**, 1729 (1996).
[19] J. C. Boettger, Phys. Rev. B **55**, 11202 (1997).
[20] N. Mounet and N. Marzari, Phys. Rev. B **71**, 205214 (2005).
[21] N. H. Dung, L. Zhang, Z. Q. Ou, L. Zhao, L. van Eijck, A. M. Mulders, M. Avdeev, E. Suard, N. H. van Dijk, and E. Brück, Phys. Rev. B **86**, 045134 (2012).
[22] G. Kresse and J. Furthmuller, Phys. Rev. B **54**, 11169 (1996).
[23] J. P. Perdew, K. Burke, and M. Ernzerhof, Phys. Rev. Lett. **77**, 3865 (1996).
[24] D. Cam Thanh, E. Brück, O. Tegus, J. Klaasse, and K. Buschow, J. Magn. Magn. Mater. **310**, e1012 (2007).
[25] X. F. Miao, L. Caron, P. Roy, N. H. Dung, L. Zhang, W. A. Kockelmann, R. A. de Groot, N. H. van Dijk, and E. Brück, Phys. Rev. B **89**, 174429 (2014).
[26] See Supplemental Material at http://link.aps.org/supplemental/10.1103/PhysRevB.93.094110 for the magnetic ordering and the atomic positions in modeled PM phase.
[27] L. Fast, J. M. Wills, B. Johansson, and O. Eriksson, Phys. Rev. B **51**, 17431 (1995).
[28] D. Bolef, N. Melamed, and M. Menes, J. Phys. Chem. Solids **17**, 143 (1960).
[29] R. Hill, Proc. Phys. Soc., London, Sect. A **65**, 349 (1952).
[30] T. Tsuchiya and K. Kawamura, J. Chem. Phys. **117**, 5859 (2002).
[31] F. Guillou, G. Porcari, H. Yibole, N. van Dijk, and E. Brück, Adv. Mater. **26**, 2671 (2014).
[32] F. Guillou, H. Yibole, N. van Dijk, and E. Brück, J. Alloys Compd. **632**, 717 (2015).
[33] F. Guillou, H. Yibole, N. van Dijk, L. Zhang, V. Hardy, and E. Brück, J. Alloys Compd. **617**, 569 (2014).
[34] O. L. Anderson, J. Phys. Chem. Solids **24**, 909 (1963).
[35] S. F. Pugh, Philos. Mag. **45**, 823 (2009).
[36] F. Giustino, *Materials Modelling using Density Functional Theory: Properties and Predictions* (Oxford University Press, Oxford, 2014).